Soft Matter

Accepted Manuscript

ROYAL SOCIETY OF CHEMISTRY

www.rsc.org/softmatter

A new lattice Monte Carlo simulation for dielectric saturation in ion-containing liquids

Xiaozheng Duan[1] and Issei Nakamura[1,*]

[1]*State Key Laboratory of Polymer Physics and Chemistry, Changchun Institute of Applied Chemistry, Chinese Academy of Sciences, Changchun, Jilin 130022, China*

(Dated: March 17, 2015)

We develop a new, rapid method for the lattice Monte Carlo simulation of ion-containing liquids that accounts for the effects of the reorganization of solvent dipoles under external electrostatic fields. Our results are in reasonable agreement with the analytical solutions to the dielectric continuum theory of Booth for single ions, ion pairs, and ionic cross-links. We also illustrate the substantial disparity between the dielectric functions for like and unlike charges on the nanometer scale. Our simulation rationalizes the experimental data for the dependence of the bulk dielectric value of water on ion concentrations in terms of saturated dipoles near ions.

PACS numbers:

I. INTRODUCTION

Ion-containing materials are ubiquitous in nature. Their biological and environmental importance have been areas of focus for many decades; however, a vast array of literature has also emerged on the study of recently developed electrochemical devices, such as lithium-ion polymer batteries, electroactive actuators, and fuel cells. However, both modeling the complex nature of electrostatic interactions and enhancing computational performance in the simulations remain key challenges commonly addressed in these studies. Importantly, recent studies based on mean-field theories have revealed that the solvent polarization near ions crucially affects the dielectric response of pure liquids [1, 2], simple liquid mixtures [3], polymer blends and block copolymer melts [4, 5].

Among others, spatially inhomogeneous dielectric responses still pose a significant challenge in both theory [3] and simulation [6, 7] despite their critical significance. First, the dielectric response of ion-containing liquids cannot be simply captured by a single parameter ε_r (i.e., the bulk dielectric constant) in the Coulomb potential, $e/(4\pi\varepsilon_0\varepsilon_r r)$, because the effects of the relative coordination among ions and solvents on the dielectric response are not considered. In other words, the effects of the multi-body forces are largely ignored in implicit solvent models. Indeed, Gong and Freed demonstrated the significant disparity between the dielectric screening functions for like and unlike charges in aqueous solutions through the application of Langevin-Debye theory [8]. Moreover, the synergistic effects of the electrostatic fields near the ion pairs in block copolymer melts cause considerably non-monotonic variations in the dielectric functions and volume fractions at the nanometer scale [5]. Second, the long-range interaction via $1/r$ often demands the Ewald summation. However, this method results in a significant cost of computational performance. Although this drawback can be considerably improved by the local lattice simulation algorithms for electrostatic interactions [9, 10], the reorganization of solvent dipoles remains elusive. Indeed, the existing simulations for the charged systems primarily draw upon a single parameter ε_r, which does not adequately account for the effects of electrostatic fields that reorient the solvent dipoles, called "dielectric saturation." Importantly, recent mean-field theories have suggested that the effects of the dipole reorientation near ions cause a decrease in the bulk dielectric constant [11–13]. This result rationalizes certain experimental values [14] but is also likely to await a fundamental breakthrough for the strategy of the simulations.

In this paper, we demonstrate our new lattice Monte Carlo (MC) simulation that accounts for the reorganization of dipoles near ions in a dielectric medium, using an aqueous solution as an example. In the resulting figures, we show systematic errors due to the lattice discretization using horizontal bars. In Sec. II, we incorporate the Booth equation into the local simulation algorithm [9, 10], which accounts for the effects of fluctuations and correlations caused by the electrostatic interaction beyond mean-field theories such as the Poisson-Boltzmann theory, to solve the Poisson equation with local dielectric functions. In Sec. III, we compare our simulation results with the analytical results of the dielectric continuum theory of Booth for single ions, ion pairs, and ionic cross-links. The reasonable agreement between the results of the theory and simulation suggests that our lattice MC simulation should be applicable to various ion-containing systems in which the dielectric response of ion-containing liquids is unlikely to be simply captured by the bulk dielectric constant. As an example application of our simulation, we evaluate the bulk dielectric constant of aqueous solutions at high ionic concentrations. In Sec. IV, we briefly summarize our results and offer some concluding remarks.

*Electronic address: nakamura@ciac.ac.cn

II. THEORY AND SIMULATION

We start with the electrostatic energy in the generic form,

$$U_{\rm el}[\vec{D}] = \int d\vec{r}\,\frac{[\vec{D}(\vec{r})]^2}{2\varepsilon_0\varepsilon_r(\vec{r})}, \tag{1}$$

where ε_0 and $\varepsilon_r(\vec{r})$ are the vacuum permittivity and local dielectric value, respectively. $\vec{D}(\vec{r})$ is the electric displacement field given by the solution of the Poisson equation, $\mathrm{div}\vec{D}(\vec{r}) = \rho(\vec{r})$, where $\rho(\vec{r})$ is the local charge density. $\varepsilon_r(\vec{r})$ should depend on the polarization of local compositions at the position $\vec{r}$. In our theory, we write $\varepsilon_r(\vec{r})$ using the Booth equation, which accounts for the reorganization of solvent dipoles under external electrostatic fields [15], in the form of $\varepsilon_r(\vec{r}) = n^2 + a_0 L(a_1)$, where n and $L(x)$ are the optical refractive index of the solvent and the Langevin function, $L(x) = 1/\tanh x - 1/x$, respectively. The coefficients a_0 and a_1 are given by $a_0 = \alpha n_0(n^2+2)\mu/[4\varepsilon_0|\vec{E}(\vec{r})|]$ and $a_1 = \beta\mu(n^2+2)|\vec{E}(\vec{r})|/(k_BT)$, respectively. n_0 is the number density of solvent, μ is the intrinsic dipole moment of the solvent, and $\vec{E}(\vec{r})$ is the electrostatic field. For water molecules, we employ $\alpha = 28/(3\sqrt{73})$ and $\beta = \sqrt{73}/6$, which account for the nonlinear dielectric responses caused by both the strong reorganization of the dipoles and the effects of hydrogen bonding [15]. Here, we employ $\vec{D}(\vec{r}) = \varepsilon_0\varepsilon_r(\vec{r})\vec{E}(\vec{r})$ to write $\varepsilon_r(\vec{r})$ in the Booth equation as a functional of $|\vec{D}(\vec{r})|$.

The ion positions are denoted by $\vec{R}_i$. The statistical ensemble of S is then given by

$$\langle S\rangle = \frac{\int\prod_i d\vec{R}_i S\exp\{-U_0 - U_{\rm el}[\vec{D}]\}}{\int\prod_i d\vec{R}_i\exp\{-U_0 - U_{\rm el}[\vec{D}]\}}, \tag{2}$$

where U_0 represents non-electrostatic interactions such as a hard-core potential. The Boltzmann factor for $U_{\rm el}[\vec{D}]$ can be written as a functional integral over an auxiliary field variable $\vec{A}(\vec{r})$ by the identity [9, 10]

$$\exp(-U_{\rm el}[\vec{D}]) = Z_{\rm fluc}^{-1}(\{r_i\})\int\mathcal{D}\vec{A}\left\{\prod_{\vec{r}}\delta[\mathrm{div}\vec{A}(\vec{r}) - \rho(\vec{r})]\right\} \times \exp(-U_{\rm el}[\vec{A}]). \tag{3}$$

Here, $Z_{\rm fluc}$ is given by the functional integration over the transverse vector $\vec{A}_t(\vec{r})$, $\int\mathcal{D}\vec{A}_t\{\prod_r\delta[\mathrm{div}\vec{A}_t]\}\exp(-U_{\rm el}[\vec{A}_t])$, where $\vec{A}_t(\vec{r}) = \vec{A}(\vec{r}) - \vec{D}(\vec{r})$. For homogeneous dielectric media, $Z_{\rm fluc}$ is constant and therefore thermodynamically inconsequential [9]. For inhomogeneous dielectric media, the fluctuation potential in $Z_{\rm fluc}$ was estimated to vary as $1/r^6$ [16]. In our coarse-grained model, this term is absorbed into U_0. By comparing the simulation results with the analytical results, we demonstrate that this treatment is reasonable.

Using Eq. (3), the statistical average of S can be cast into the form

$$\langle S\rangle = \int\prod_{\vec{r}} d\vec{R}_i\mathcal{D}\vec{A}\left\{\prod\delta[\mathrm{div}\vec{A}(\vec{r}) - \rho(\vec{r})]\right\}S \times \exp\{-U_0 - U_{\rm el}[\vec{A}]\}/\int\prod_{\vec{r}} d\vec{R}_i\mathcal{D}\vec{A} \times \left\{\prod\delta[\mathrm{div}\vec{A}(\vec{r}) - \rho(\vec{r})]\right\}\exp\{-U_0 - U_{\rm el}[\vec{A}]\} \tag{4}$$

$\varepsilon_r[\vec{A}(\vec{r})]$ in $U_{\rm el}[\vec{A}]$ is not the physical dielectric value at the position $\vec{r}$ but purely a functional of $\vec{A}(\vec{r})$. Note that the transverse vector, $\vec{A}_{\rm tr}(\vec{r}) = \vec{A}(\vec{r}) - \vec{D}(\vec{r})$. We then obtain $\langle\mathrm{div}\vec{A}_{\rm tr}(\vec{r})\rangle = Z_0^{-1}\int\prod d\vec{R}_i D\vec{A}_{\rm tr}\,\delta[\mathrm{div}\vec{A}_{\rm tr}(\vec{r})]\mathrm{div}\vec{A}_{\rm tr} \times \exp\{-U_0 - U_{\rm el}[\vec{A}_{\rm tr}]\} = 0$, which leads to $\langle\mathrm{div}\vec{A}(\vec{r})\rangle = \rho(\vec{r})$ and hence $\vec{D} = \langle\vec{A}(\vec{r})\rangle$. Here, Z_0 denotes the normalization factor in Eq. (4). The physical dielectric function $\varepsilon_r(\vec{r})$ can be calculated from $\langle\vec{A}(\vec{r})\rangle$ using the Booth equation.

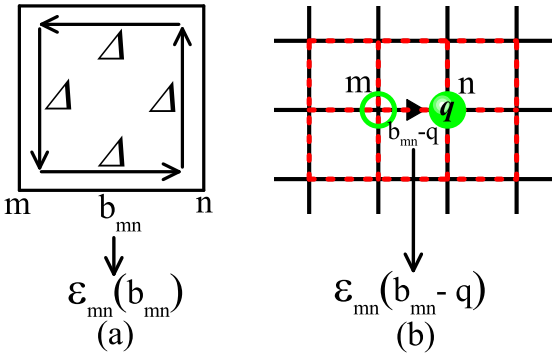

FIG. 1: Schematic illustration of the local algorithm for the Monte Carlo updates. (a) Updates of the lattice variable b_{mn} and dielectric value ε_{mn} on the bond connecting site m to site n. When b_{mn} is increased by a random value Δ, all other lattice variables on the plaquette are also increased by Δ in the direction of the arrows; the dielectric value ε_{mn} is then calculated from the new b_{mn} using the Booth equation. (b) Updates for the position of an ion. When an ion with charge q moves from site m to site n, b_{mn} is shifted to $b_{mn} - q$. Accordingly, ε_{mn} is calculated from $b_{mn} - q$ using the Booth equation. We then perform the procedure described in panel (a) on the red-dashed plaquettes near the ion, which relaxes a large activation barrier to move ions.

We now perform the MC simulation for Eq. (4) on a lattice with a three-dimensional periodic boundary condition in the NVT ensemble using the local simulation algorithm. Interested readers refer to the detail of the algorithm in, for example, Refs. [9], [17], [18], and [10]. In this study, we describe the essential difference in the algorithm, which arises from the effects of the reorganization of solvent dipoles, from that used in the previous studies.

Ions are modeled as a particle with charge q situated on the lattice grid. Empty sites correspond to a spatial point in the dielectric continuum whose constituent consists of solvent with a dipole moment $\vec{\mu}$. Thus, our lattice model approaches the dielectric continuum as the lattice spacing is decreased. In other words, our lattice discretization indicates the spatial resolution to solve the Poisson equation. By applying the discrete version of the integral form of the Poisson equation (the Gauss theorem) to a cube of the lattice bond length, which encloses site m, we obtain $\Sigma_n b_{mn} = q_m$, where n denotes the nearest neighbors of site m, q_m is the charge on site m, and the lattice variable b_{mn} is the current of the vector $\vec{A}$ through a surface of the cube that bisects the lattice bond connecting m and n. To account for the effects of saturated dipoles caused by local electrostatic fields from the ions, we associate the dielectric value ε_{mn} to the lattice bond with lattice variable b_{mn} using the Booth equation; see Fig. 1 (a) for a schematic explanation of the algorithm. The Monte Carlo sampling then involves initializing a set of b_{mn} for all of the lattice bonds at a given charge distribution, followed by sequential updating of the group of b_{mn} on a plaquette. Importantly, this update scheme always satisfies the Gauss theorem $\sum_n b_{mn} = q_m$ at all four vertices. We determine the acceptance and rejection of the MC updates using the Metropolis algorithm through the Boltzmann weighting factor $\exp(-U_0 - U_{\rm el}[\vec{A}])$.

The position update of each ion also includes the updates of the lattice variable and the dielectric value assigned to the bond connecting the old and new positions of the ion [9]. To enhance the efficiency of the MC updates, we thermalized the lattice variables on the red-dashed plaquettes near the old and new positions of the ion; see Fig. 1(b). This treatment relaxes a relatively large activation barrier in the MC updates that is caused by the change in the lattice variable and hence the dielectric value. In this study, we have repeated this thermalization 100 times for each movement of the ion.

We consider single ions, ion pairs, and ionic cross-links, performing the order of 10^8 steps for the MC updates of the auxiliary fields. The lattice units are set to $u = 2.8$, 1.4, and 0.7 Å. The size of the simulation box ranges from $L^3 = (10u)^3$ to $L^3 = (40u)^3$. For ionic solutions, we perform the order of 10^9 for the MC updates of the auxiliary fields. According to the size of the simulation box from $L^3 = (10u)^3$ to $L^3 = (40u)^3$, each simulation took 2-24 hours by our Dell Precision T5610 workstation (Intel Xeon E5-2650 v2, 2.6 GHz CPU, and 16GB Memory). To obtain the statistical ensemble, we employed computer clusters at our institute and Computing Center of Jilin Province. These two resources provided us with approximately the order of hundreds of cores. Within this computational performance, our computation time was reasonable. If one encounters larger system sizes or low-dielectric media, improved simulation algorithms could also be used [17, 19]. We perform the statistical analysis by averaging the order of 10^3 samples. Along the same lines in Ref. [12], we calculate the bulk dielectric constant, ε_r, by averaging the dielectric function $\varepsilon_r(\vec{r})$ over a sphere with radius of R around each ion, where $R = [3/(4\pi c)]^{1/3}$ denotes the mean distance between ions in ion concentration c.

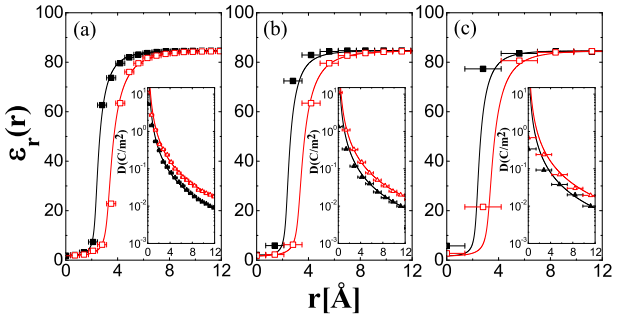

FIG. 2: Dielectric function $\varepsilon_r(r)$ and electric displacement $D(r)$ (insets) for single ions. r is the distance from the ion. The colors of the lines and symbols correspond to monovalent (black) and divalent (red) ions, respectively. The lines and symbols denote the analytical results and simulation results, respectively. The lattice unit u is set to (a) 0.7 Å, (b) 1.4 Å, and (c) 2.8 Å.

III. RESULTS

We first illustrate the remarkable agreement between the analytical results and simulation results. The electric displacement field arising from an ion at the position $\vec{r}_0$ is given by $|\vec{D}(\vec{r})| = qe/[4\pi\varepsilon_0(\vec{r} - \vec{r}_0)^2]$. By solving the Booth equation with this equation and $\vec{E}(\vec{r}) = \vec{D}(\vec{r})/[\varepsilon_0\varepsilon_r(\vec{r})]$, we can obtain the analytical results of the dielectric function $\varepsilon_r(\vec{r})$ as the solution of the dielectric continuum model. In Fig. 2, we compare the simulation results of $\varepsilon_r(\vec{r})$ and $\vec{D}(\vec{r})$ with the analytical results. Our lattice simulation largely reproduces the dielectric continuum theory of Booth for both monovalent and divalent ions. The results are qualitatively robust even when the lattice unit is relatively large with $u = 2.8$ Å. Incidentally, our results for the dielectric saturation are also consistent with those derived from the Langevin-Debye theory [20, 21].

Of particular interest in ion-containing liquids is the solvation of ion pairs [22]. We set the origin of the r axis in the middle of the two ions. The superposition principle and spherical symmetry of the electric displacement fields around the ions lead to $|\vec{D}(\vec{r})| = |\vec{D}_1(\vec{r}) + \vec{D}_2(\vec{r})| = \sqrt{|\vec{D}_1|^2 + |\vec{D}_2|^2 + 2|\vec{D}_1||\vec{D}_2|\cos\varphi_\pm}$, where φ_+ for like charges and φ_- for unlike charges denote the angles between $\vec{D}_1$ and $\vec{D}_2$, with $\varphi_- = \pi - \varphi_+$ [5]. Using this formula, we can solve the Booth equation analytically. Because the resultant analytical solutions of the dielectric function exhibit unconventional behaviors, before the demonstration of our simulation, we first illustrate them in Fig. 3 (a). The marked difference be-

tween the dielectric functions for like and unlike charges appears near the center ($r = 0$); $\varepsilon(\vec{r})$ of the like charges (black and red dashed lines) exhibits a drastic spiky variation between the ions, whereas the variation in $\varepsilon(\vec{r})$ of the unlike charges (black and red solid lines) is relatively small. The former case is caused by the fact that the electric displacement fields are significantly weakened near $\varphi_+ = \pi$. However, $\varepsilon(\vec{r})$ of the unlike charges remains small between the charges because the electric displacement fields tend to be strengthened near $\varphi_- = 0$. This nature of the dielectric saturation still remains significant even when the two charges are separated by the *nanometer* scale [Fig. 3 (b)]. The substantial disparity between the dielectric functions for the like and unlike charges occurs even outside the ion pairs separated by 5.6 Å [Fig. 3 (a)]. Thus, the unlike charged pair cannot be literally regarded as a charge-neutral species in terms of the dielectric screening. This feature is consistent with highly saturated dipoles near ion pairs that have been illustrated by molecular dynamics simulations [23].

Figs. 3 (c) and (d) show the simulation results of the electric displacement field (triangles) and dielectric function (squares) between unlike charges on the r axis. These results correspond to those in Figs. 3 (a) and (b), respectively. For the significant variations in the dielectric function near the ions, we present the results for only the relevant scale between the charges. Although the sharp peak of the dielectric function in the inset of Fig. 3 (c) cannot be fully captured by the spatial resolution with the present lattice spacing, our simulation results are highly consistent with the analytical results for both monovalent and divalent ion pairs.

We write the solvation energy of an ion pair in a dielectric medium in the form of the potential mean force [8],

$$\begin{aligned}\Delta G &= G - G_1 - G_2 \\ &= \frac{1}{2}\int\int\int_V \frac{\vec{D}(\vec{r})^2}{\varepsilon_0\varepsilon_r(\vec{r})}d\tau - \frac{1}{2}\int\int\int_{V_1} \frac{\vec{D}_1(\vec{r})^2}{\varepsilon_0\varepsilon_r(\vec{r})}d\tau \\ &- \frac{1}{2}\int\int\int_{V_2} \frac{\vec{D}_2(\vec{r})^2}{\varepsilon_0\varepsilon_r(\vec{r})}d\tau,\end{aligned} \tag{5}$$

where G, G_1, and G_2 represent the energies of the two charges and independent single charges in a dielectric medium, respectively. We perform the integrations over the volumes V, V_1, and V_2, which include all space excluding the interior of the ions. $\vec{D}$, $\vec{D}_1$, and $\vec{D}_2$ represent the electric displacement fields that apply for two-charge and single-charge systems, respectively. To ensure the accuracy of the integrations, we evaluate Eq. (5) using the analytical solutions of the Booth equation instead of the results of the lattice simulations.

Our results also suggest that the effects of the dielectric saturation may substantially alter the solvation energy ΔG of unlike ion pairs. Our analysis based on the Booth equation for an ion pair separated by several

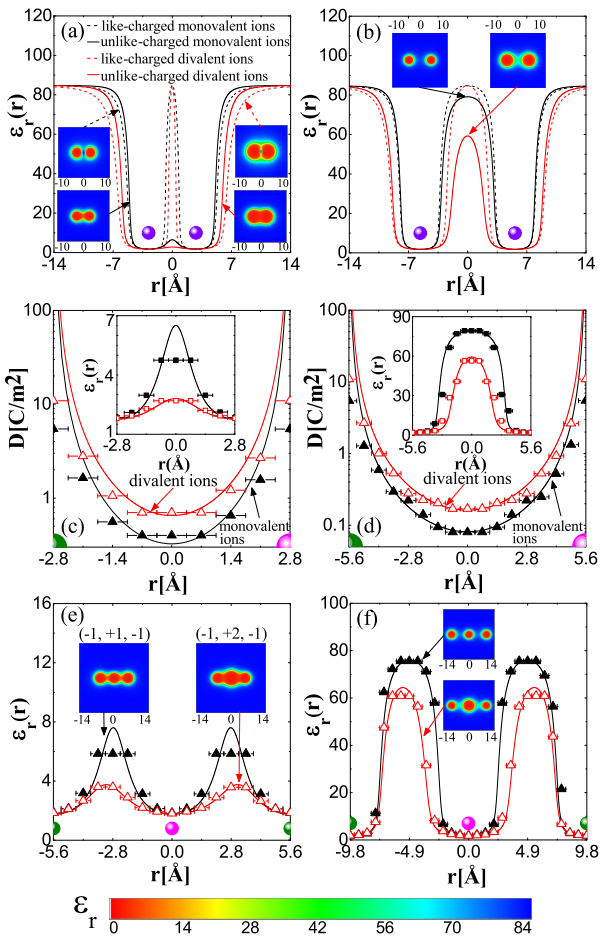

FIG. 3: (a) and (b): Analytical results of the dielectric function $\varepsilon_r(r)$ for the like charges (dashed lines) and unlike charges (solid lines), separated by a distance of (a) 5.6 Å and (b) 11.2 Å. The colors of the lines correspond to monovalent (black) and divalent (red) charges. (c) and (d): Analytical results (lines) and simulation results (triangles and squares) of $D(r)$ and $\varepsilon_r(r)$ (insets) between unlike charges. (c) and (d) correspond to (a) and (b), respectively. (e) and (f): Analytical results (lines) and simulation results (triangles) for $\varepsilon_r(r)$ of cation-centered cross-links. Two anions separated by (e) 11.2 Å and (f) 19.6 Å. The colors of the lines correspond to (q_-, q_+, q_-) = (-1, +1, -1) (black) and (-1, +2, -1) (red). The lattice unit is $u = 1.4$ Å. The r axes are set through the ions.

angstroms reveals a noticeable activation energy in ΔG (e.g., $1.6k_BT$ for Na^+ or Li^+ and Cl^- in Fig. 4) that does not appear in linear-dielectric continuum theory. The peak position and height of the energy barriers are consistent with those typically determined from quantum mechanical molecular dynamics simulations [24–28]; the energy barrier tends to vanish as ion size increases. Thus, the Booth equation captures the key qualitative features of the solvation of ion pairs. Moreover, the contribution of the hydrogen bonding to ΔG is less than 1%. Therefore, the solvation energy can be accounted for primarily by the reorganization of the dipoles in response to the electrostatic field in the vicinity of the ions. This

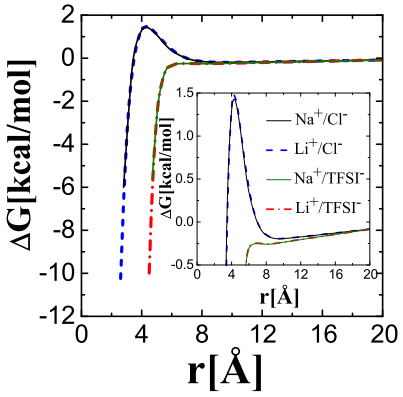

FIG. 4: Analytical results of the solvation energy ΔG for Na^+-Cl^- (black solid line), Li^+-Cl^- (blue dashed line), Na^+-$TFSI^-$ (green solid line), and Li^+-$TFSI^-$ (red dot-dashed line) as a function of the separation distance between the ions. The ionic radii of Li^+, Na^+, Cl^-, and $TFSI^-$ are 0.78 Å, 0.98 Å, 1.81 Å, and 3.81 Å, respectively. There is no distinguishable hump in the energy of ion pairs consisting of large anions such as $TFSI^-$. The inset shows an enlarged section of the plot.

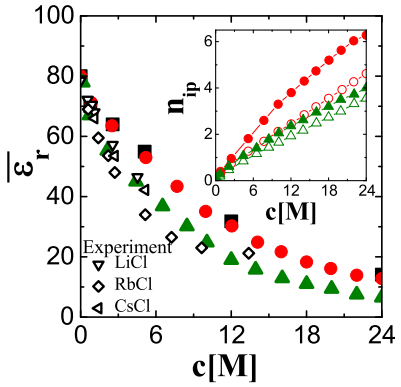

FIG. 5: Bulk dielectric constant $\bar{\varepsilon}_r$ as a function of ion concentration c. The filled and empty symbols indicate our simulation and experimental results from Ref. [14], respectively. The colors of the symbols correspond to the lattice unit, $u = 2.8$ Å (black squares and red spheres for $L = 40u$ and $10u$, respectively) and 1.4 Å (green triangles). The inset shows the number of ion pairs n_{ip} obtained from the simulation with the dielectric function $\varepsilon_r(\vec{r})$ (filled symbols) and the bulk dielectric constant $\bar{\varepsilon}_r = 80$ (empty symbols).

fact may also affect the dynamics of charge transfers or ion transports [29, 30]. In this context, electron transfer theory is likely to be altered [31]. Given the considerable interest in organic energy storages, the application of our simulation to photovoltaic cells [32] would also be of further interest.

Ionic cross-linking is another important class of complexation that may substantially alter the mechanical strength and electronic properties of electrolytes. For example, ionic complexation consisting of lithium ions and anions, such as TFSI, is the key feature to controlling ionic conductivity in salt-doped polymer membranes [29]. Thus, we consider the cross-links consisting of two anions and one cation. Again, our simulation results correspond well with the analytical results [Figs. 3 (e) and (f)]. Notably, the effects of the dielectric saturation are significant even on the nanometer scale.

With the three-body systems examined, our simulation should be able to account for the multi-body interaction that causes highly non-monotonic variations in the dielectric function. To demonstrate this fact, Fig. 5 further illustrates that our simulation rationalizes the experimental observation concerning the dependence of the ion concentration c on the bulk static dielectric constant $\bar{\varepsilon}_r$ [14]. Here, we introduced the hard-core repulsion between the ions with the ionic radius 1.4 Å as an average of that for Li^+, Rb^+, Cs^+, and Cl^-. We changed the simulation box size from $40u$ (black squares) to $10u$ (red spheres) but observed no significant effect on the results. Thus, our simulation method has the advantage of enabling fast statistical convergence using a relatively small simulation box. The systematic error due to the lattice discretization should be reduced by decreasing the lattice unit from $u = 2.8$ Å (red spheres) to $u = 1.4$ Å (green triangles). We then obtain high consistency between the simulation and experimental results; the variation in the bulk dielectric constant $\bar{\varepsilon}_r$ is primarily caused by saturated dipoles near ions causing significant decreases in $\bar{\varepsilon}_r$. Our present results support the mean-field theories [11, 12] that account for these experimental observations in terms of the saturated dipoles. In other words, the variation in $\bar{\varepsilon}_r$ is attributed to the local dielectric value lower than the dielectric constant of the salt-free system. However, our simulation further indicates substantial increases in the number of ion pairs [the inset in Fig. 5], separated on the nearest-neighbored lattice grids under the hard-core potential, which are not accounted for in the previous theories. However, given the low dielectric value of water with high salt concentrations, the formation of ion pairs is likely to be reasonable.

Finally, we demonstrate the radial distribution functions for like (g_{++}) and unlike (g_{+-}) charged ion pairs as a function of the ion concentration c [Fig. 6]. Our simulation results are qualitatively consistent with the previous results of the integral-equation theories [33] and MC simulations [34] based on the primitive model with the bulk dielectric constant $\bar{\varepsilon}_r$. However, in our simulation, the effects of the saturated dipoles yield relatively stronger electrostatic interactions, causing larger contact values of g_{+-}. Therefore, this result should motivate further in-depth studies of the effects of the dielectric inhomogeneity on the equation of states.

IV. CONCLUSION

In summary, we developed a new lattice MC method that accounts for the effects of the reorganization of solvent dipoles under external electrostatic fields. We in-

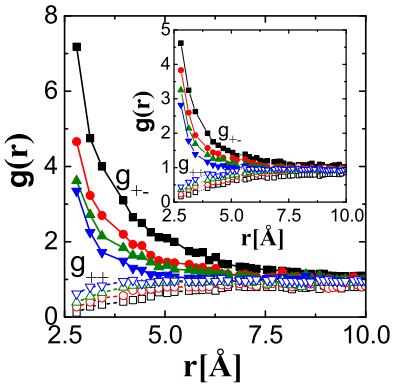

FIG. 6: The radial distribution functions for unlike and like charges. The colors of the symbols correspond to 0.70 M (black squares), 2.1 M (red spheres), 4.2 M (green triangles), and 12.0 M (blue inverse triangles). The inset shows the simulation results with the bulk dielectric constant $\bar{\varepsilon}_r$. The lattice unit is $u = 1.4$ Å.

corporated the Booth equation, which provides the local dielectric function, into the local simulation algorithm [9] to solve the Poisson equation. Our simulation results include the effects of fluctuations and correlations caused by the electrostatic interaction beyond mean-field theories such as the Poisson-Boltzmann theory. We do not encounter unphysical, dynamic traps of strongly attractive ion pairs during the simulation because of the relatively high dielectric values of water. Our method does not employ the Ewald summation and is, thus, computationally fast. We demonstrated that our simulation results correspond well with the analytical results of the dielectric continuum theory of Booth for single ions, ions pairs, and ionic cross-links [Figs. 2 and 3], being robust to changes in the simulation box size from $L = 40u$ to $L = 10u$. The functional integration over the transverse vector $Z_{\rm fluc}$ is absorbed into the non-electrostatic interaction U_0. This treatment for spatially varying dielectric values is controversial [16, 18, 35]; however, our current results suggest that $Z_{\rm fluc}$ is insignificant with regard to the effects of the dielectric inhomogeneity. We illustrated the significance of the saturated dipoles near ions and the substantial disparity between the dielectric functions for like and unlike charges. These effects may become considerably large at the nanometer scale. Our simulation results also rationalize variations in the observed bulk dielectric constant upon the addition of salt ions [Fig. 5], leading to substantial changes in the number of ion pairs. Accordingly, the effect of the saturated dipoles alters the radial distribution function particularly for unlike charged pairs [Fig. 6]. Thus, we suggest that future research focus on the effects of the dielectric saturation near the strongly correlating ions on the phase behavior of ion-containing liquids [36].

Finally, the effects of the reorganization of dipoles cause noticeable activation energy (e.g., $1.6k_BT$ for Na^+ or Li^+ and Cl^-) of ion pairing in aqueous solutions (Fig. 4). Given this situation, we suggest that the dynamic property of ion-containing liquids is affected by the saturated dipoles [37]. Similarly, the electron transfer in photovoltaic cells would also be of particular interest, because the recombination rate of electrons and holes is critical to enhancing the energy efficiency [38].

This work was supported by the National Natural Science Foundation of China (21474112, 21404103). We are grateful to Computing Center of Jilin Province for essential support.

[1] R. D. Coalson and A. Duncan, J. Phys. Chem. **100**, 2612 (1996).
[2] A. Abrashkin, D. Andelman, and H. Orland, Phys. Rev. Lett. **99**, 077801 (2007).
[3] I. Nakamura, A. C. Shi, and Z.-G. Wang, Phys. Rev. Lett. **109**, 257802 (2012).
[4] I. Nakamura, J. Phys. Chem. B **118**, 5787 (2014).
[5] I. Nakamura, Soft Matter **10**, 9596 (2014).
[6] K. Barros and E. Luijten, Phys. Rev. Lett. **113**, 017801 (2014).
[7] M. Sega, S. S. Kantorovich, C. Holm, and A. Arnold, J. Chem. Phys. **140**, 211101 (2014).
[8] H. P. Gong and K. F. Freed, Phys. Rev. Lett. **102**, 057603 (2009).
[9] A. C. Maggs and V. Rossetto, Phys. Rev. Lett. **88**, 196402 (2002).
[10] I. Nakamura and Z. G. Wang, Soft Matter **9**, 5686 (2013).
[11] B. Maribo-Mogensen, G. M. Kontogeorgis, and K. Thomsen, J. Phys. Chem. B **117**, 10523 (2013).
[12] A. Levy, D. Andelman, and H. Orland, Phys. Rev. Lett. **108**, 227801 (2012).
[13] A. Levy, D. Andelman, and H. Orland, J. Chem. Phys. **139**, 164909 (2013).
[14] Y. Z. Wei, P. Chiang, and S. Sridhar, J. Chem. Phys. **96**, 4569 (1992).
[15] F. Booth, J. Chem. Phys. **19**, 391 (1951).
[16] A. C. Maggs, J. Chem. Phys. **120**, 3108 (2004).
[17] L. Levrel and A. C. Maggs, Phys. Rev. E **72**, 016715 (2005).
[18] J. Rottler and A. C. Maggs, Soft Matter **7**, 3260 (2011).
[19] A. Duncan, R. D. Sedgewick, and R. D. Coalson, Phys. Rev. E **71**, 046702 (2005).
[20] A. K. Jha and K. F. Freed, J. Chem. Phys. **128**, 034501 (2008).
[21] H. P. Gong, G. Hocky, and K. F. Freed, Proc. Natl. Acad. Sci. U. S. A. **105**, 11146 (2008).
[22] Y. Marcus, J. Phys. Chem. B **109**, 18541 (2005).
[23] C. J. Fennell, A. Bizjak, V. Vlachy, and K. A. Dill, J. Phys. Chem. B **113**, 6782 (2009).
[24] B. Hess, C. Holm, and N. van der Vegt, Phys. Rev. Lett. **96**, 147801 (2006).
[25] S. Gavryushov, J. Phys. Chem. B **110**, 10888 (2006).
[26] S. Gavryushov and P. Linse, J. Phys. Chem. B **110**, 10878 (2006).

[27] P. J. Lenart, A. Jusufi, and A. Z. Panagiotopoulos, J. Chem. Phys. **126**, 044509 (2007).
[28] Y. Luo, W. Jiang, H. B. Yu, A. D. MacKerell, and B. Roux, Faraday Discuss. **160**, 135 (2013).
[29] O. Borodin and G. D. Smith, Macromolecules **39**, 1620 (2006).
[30] M. Mirzadeh, F. Gibou, and T. M. Squires, Phys. Rev. Lett. **113**, 097701 (2014).
[31] R. A. Marcus, J. Chem. Phys. **24**, 966 (1956).
[32] G. A. Buxton and N. Clarke, Model. Simul. Mater. Sci. Eng. **15**, 13 (2007).
[33] J. C. Rasaiah, J. P. Valleau, and D. N. Card, J. Chem. Phys. **56**, 248 (1972).
[34] D. N. Card and J. P. Valleau, J. Chem. Phys. **52**, 6232 (1970).
[35] A. Duncan, R. D. Sedgewick, and R. D. Coalson, Phys. Rev. E **73**, 016705 (2006).
[36] C. E. Sing, J. W. Zwanikken, and M. O. de la Cruz, Phys. Rev. Lett. **111**, 168303 (2013).
[37] K. F. Rinne, S. Gekle, and R. R. Netz, J. Chem. Phys. **141**, 214502 (2014).
[38] J. Szmytkowski, Chem. Phys. Lett. **470**, 123 (2009).